ALKALI ATTACK OF COAL GASIFIER REFRACTORY LININGS

by

Tawei Sun

Thesis submitted to the Faculty of the

Virginia Polytechnic Institute and State University

in partial fulfillment of the requirements for the degree of

MASTER OF SCIENCE

in

Materials Engineering

APPROVED:

J. J. Brown, Jr.

D. Farkas

J. L. Lytton

June, 1986
Blacksburg, Virginia

ALKALI ATTACK OF COAL GASIFIER REFRACTORY LININGS

by

Tawei Sun

Committee Chairman: Jesse J. Brown
Materials Engineering

(ABSTRACT)

Thermodynamic calculations are used to study the alkali reactions in coal gasifier atmospheres. The reactive alkali and sulfur species released from coal are first calculated at temperatures from 800 K to 1900 K and pressures from 1 atm to 100 atm. Four P-T diagrams are constructed for the stable alkali and/or alkali-sulfur species at different temperatures and pressures. Alkali vapors are generated by the reactions

$$Na_2CO_{3(s)} + 2C_{(s)} = 2Na_{(g)} + 3CO_{(g)}$$

$$Na_2CO_{3(s)} + H_2O_{(g)} + C_{(s)} = 2NaOH_{(g)} + 2CO_{(g)}$$

or

$$K_2CO_{3(s)} + 2C_{(s)} = 2K_{(g)} + 3CO_{(g)}$$

$$K_2CO_{3(s)} + H_2O_{(g)} + C_{(s)} = 2KOH_{(g)} + 2CO_{(g)}$$

The phases formed from alkali-cement, and alkali-sulfur-cement reaction are also predicted. For both 53% and 72% alumina cement, calcium aluminate ($CaO \cdot Al_2O_3$) is decomposed by the reactions

$$CaO \cdot Al_2O_3 + 2Na + 1/2O_2 = Na_2O \cdot Al_2O_3 + CaO$$

$$CaO \cdot Al_2O_3 + 2K + 1/2O_2 = K_2O \cdot Al_2O_3 + CaO$$

or

$$CaO \cdot Al_2O_3 + 2Na + 1/2S_2 = Na_2O \cdot Al_2O_3 + CaS$$

$$CaO \cdot Al_2O_3 + 2K + 1/2S_2 = K_2O \cdot Al_2O_3 + CaS$$

Acknowledgements

I would like to thank Dr. Jesse J. Brown for so many things, in essence, for his trust, a driving force for people to be responsible. I am also indebted to Dr. Diana Farkas for giving her precious weekend time in discussion, and to Dr. Jack L. Lytton for serving on the committee.

Special thanks are given to a special person, Nancy Brown, for the multiroles she played.

Table of Contents

List of Tables

List of Figures

I. Introduction

Alkali-attack is a common problem in many high temperature technologies where the presence of alkali is usually encountered. For instance, soda is a major raw material in making glass, alkali impurities are almost always present in blast furnaces, and alkali species are ubiquitous in coal conversion and coal combustion systems. For some cases, alkali species are present as additives. This includes their role as electron sources in the magnetohydrodynamic (MHD) combustion system,[1] or as catalysts for coal gasifying processes to lower the gasifier operating temperature and increase the shift-methanation temperature,[2] or as an absorbing medium. However, in most combustion systems, the presence of alkali is undesirable. This is particularly true in fossil energy systems.

Coal gasification involves the production of synthetic or substitute natural gas (SNG) from coal. On combustion, alkali species are released from coal. When refractories are exposed to the alkali atmosphere, a series of reactions may occur, which either degrades the refractory materials, or causes premature failure. For most refractory systems, the presence of alkali tends to lower the liquidus temperature and results in localized melting. Alternatively, compounds with lower densities often form when alkali reacts with refractory linings. These compounds tend to spall off when subjected to thermal cycling. In certain cases where the atmosphere is rich in steam, the hydration-dehydration cycle of the alkali compound formed will add to the spalling of refractory material. It is also known that alkali impurities

decrease the viscosity of silicate melts; therefore, refractories with high silica contents may show gradual softening after long exposure to the alkali atmosphere. Porosity is another factor usually related to alkali corrosion. Either by alkali melt infiltration or alkali vapor penetration through the pores, alkali attack is no longer confined to the surface. Instead, it can penetrate below the surface, depending on the pore structure, and cause even more severe problems.

In addition to alkali, sulfur is also constantly present in coal gasifiers. For calcium aluminate bonded refractory castables, which are almost exclusively used as non-slagging gasifier linings, the presence of sulfur impurities can result in sulfur corrosion. Sulfur impurities have been found to preferentially attack the calcium aluminate bonding phase of refractory castables by forming calcium sulfide.[3] The sulfidation of lime and iron oxide will lead to substantial volume change due to the significant difference in densities between oxides and sulfides. It appears that sulfur and alkali impurity may act synergistically in attacking the gasifier linings, and lead to a dramatic reduction in the durability of refractory linings.

The mechanism and the state of the release of alkali and sulfur impurities from coal are poorly understood. Experimental identifications of the species existing in the gasifier atmosphere are extremely difficult due to the combined aggressive conditions of high temperature, high pressure, and high chemical reactivity in coal gasification atmospheres. In order to understand the release of alkali and sulfur, a thermodynamic approach is adopted in the present study to calculate the equilibrium states of these impurities under the coal gasification

atmosphere using the SOLGASMIX-PV computer program. The SOLGASMIX-PV is capable of calculating chemical equilibrium at various temperatures and pressures. Phases formed from the reactions of alkali and/or alkali-sulfur impurities with the gasifier linings are also predicted by thermodynamic calculations. Results from these calculations are partially compared with experimental results. Investigations should concentrate on the bonding phase of refractory castables, because it was found that corrosion started at the bonding phase and the aggregate remained largely unreacted. Therefore, the present study involves:

1. Calculation of equilibrium alkali and sulfur species existing in the coal gasification atmosphere,
2. Calculations of the phases formed from the reactions of alkali and/or alkali-sulfur impurity with alumina cement.

II. Related Literature

A. Background Information

Results of laboratory tests and analyses of degraded refractory materials after exposure to alkali environments are reported by various authors. Rigby and Hutton carried out a series of tests to study the reactions of alkali and alkali-vanadium oxide with alumina-silica refractories.[4] In their tests, samples with different alumina contents ranging from pure silica to pure alumina were prepared, and then ground and mixed with sodium carbonate. The powder mixtures were pressed and fired at successive temperatures from 800°C to 1600°C, or until melting occurred. Samples corresponding to silica brick melted near 800°C after reactions, and samples with compositions close to fireclay brick melted at 1000°C. When the alumina content was increased to that approaching the composition of commercial silimanite brick, soda first attacked the excess alumina by forming sodium aluminate, and then decomposed mullite by forming nepheline. Volume expansion was noted for this reaction. Similar results, but larger volume expansions were found for the sample corresponding to 80% alumina brick. For pure alumina, soda reacted to form sodium aluminate or β-alumina at and above 1300°C. It was concluded that when the alumina content was less than that in mullite, soda first attacked silica to form sodium silicate, and then began to decompose mullite with the formation of nepheline. A low eutectic melt was associated with this reaction, which resulted in shrinkage due to liquid formation. In the high silica corner of the Na_2O-Al_2O_3-SiO_2 phase diagram, a eutectic liquid forms at temperatures

as low as 732°C. When the alumina content was above the mullite composition, soda first reacted with alumina to form sodium aluminate before decomposing mullite to form nepheline. The formation of sodium aluminate or β-alumina can cause a large volume expansion. The theoretical volume expansions corresponding to the formation of sodium aluminate and β-alumina are 14% and 20%, respectively. When vanadium oxide was present together with soda, the reactions proceeded faster, since sodium vanadate acts both as a flux and mineralizer in forming sodium aluminum silicate.

Similar tests, but at a lower alkali concentration, were made by Farris and Allen, including both soda and potassia reactions with 42% to 90% alumina refractories.[5] Samples were ground and mixed with sodium carbonate and potassium carbonate, respectively. The testing temperatures ranged from 870°C to 1430°C. Both nepheline and a sodium aluminum silicate with either a 3:2:4 or 2:1:2 soda-alumina-silica ratio were found. The amount of nepheline formed decreased with increasing alumina content, and virtually disappeared for the 70% high-fired and 90% alumina samples. The amount of the 3:2:4 or 2:1:2 sodium aluminum silicate formed increased with increasing temperature. This high soda, low silica compound (3:2:4 or 2:1:2 sodium aluminate silicate) exists as the amount of soda increases or as silica decreases. Beta alumina also formed at high temperature while sodium aluminate was not a common product as was the case in Rigby and Hutton's study. This is due to the relatively low soda content used in Farris and Allen's tests. When soda was replaced by potassia, kaliophilite and leucite were the most common reaction products. The attack sequence began at

the glass matrix, or cristobalite, and progressed to the fine crystalline mullite, and finally to the coarser mullite. X-ray analyses showed that cristobalite was immediately depleted at low temperatures (~ 850°C). The amount of mullite decreased with increasing temperature and eventually disappeared at high temperatures. It was also concluded that free alumina was least attacked by alkali.

The failure of the coal gasifier lining at Grand Forks Energy Technology Center best demonstrates the consequence of alkali attack, where the gasifier cracked and spalled after exposure to the coal gasification atmosphere for a total of only about 125 hours at a hot face temperature of 1000 ± 200°C.[6] The gasifier was lined with high grade mullite tile backed by insulating firebrick and insulating refractory castable. X-ray analyses of the exposed lining indicated that mullite had been almost completely converted to carnegieite and beta alumina. Failure occurred as a result of the volume expansion associated with this reaction.

Shapland and Livovich tested refractory castables made from different calcium aluminate cements.[7] Their results showed that the castables tested had poor resistance to alkali attack; all specimens cracked after one cycle in the alkali cup test.

Blast furnaces are in many ways similar to coal gasifiers. McCune et al. studied the peeling of fireclay and 70% alumina brick in blast furnace atmospheres, where the potassia concentration was found to be as high as 30% in certain regions.[8] Testing methods included spreading potassium carbonate on the brick surface and mixing potassium carbonate with the ground samples. Results showed that deep cracks appeared on

the surface of 70% alumina brick, while fireclay brick maintained surface integrity. This is due to the surface glaze of fireclay brick which seals the surface pores and prevents the penetration of molten potassium carbonate. X-ray analyses of the powder mixtures after reactions showed the presence of leucite and kaliophilite. It was also found that cristobalite was the first constituent attacked by alkali. Samples taken from the blast furnace were also analyzed, and alkali attack was found in two different forms in the lining. In the first form, usually less than 10% K_2O is present and the hot face of the altered brick has a relatively dense, hard, glassy structure. In the second form, the K_2O content is between 15 and 30%. The hot face of the altered brick is a thinly laminated, light-colored crystalline material having a higher apparent porosity and lower bulk density than other portions of the brick. It seems that the second form is only the end product of the first when enough alkali is present, and the peeling is attributed to the formation of leucite and kaliophilite.

A further investigation of alkali attack on blast furnace linings was carried out using the alkali cup test in a controlled CO/CO_2 atmosphere to simulate blast furnace conditions.[9] Both 45% and 60% alumina castables showed relatively good resistance to alkali attack at 1200°C, but large volume expansion occurred at 1400°C. The volume expansions associated with the formation of kaliophilite and leucite from fireclay were 6% and 10%, respectively. The conversion of corundum to beta alumina ($KAl_{11}O_{17}$) results in a 15% volume increase. Thermogravimetric analyses indicated that reactions started at a temperature as low as 500°C. Thermodynamic calculations showed that the reacting potassium

species in the controlled CO/CO_2 atmosphere is potassium vapor above 1200 K, and potassium carbonate below 1200 K.

The failure of checker brick in glass tank regenerators is another example of alkali attack, where alkali pick-up or absorption causes peeling of the refractory lining. Analysis of the failed surface showed absorption of large amount of soda. The deposit formed on the surface was principally composed of nepheline, carnegieite, and corundum.[10] Unequal temperature distributions set up stresses between the core and outer shell of the brick, which consequently cause separation of the less dense material from the body.[11] Petrie and Brown found a 1/4 in. to 1/2 in.-thick shell partially separated from the body of the checker brick.[12] If the absorption continues, as one layer becomes loosened, another starts to form. The shelling may continue until the bricks are completely destroyed in certain zones of the regenerator. In addition, the presence of alkali impurities can lower the fusion point of the hot face as was found in many oil-fired furnaces.[13-14]

The presence of sulfur impurities can be particularly damaging to refractory castables. In view of the high stability of CaS, the calcium aluminate bonding phase may be preferentially attacked by the sulfur species. Eight castables of compositions from 40% to 96% alumina were tested by Tak and Young in a controlled sulfur atmosphere.[3] Results showed that the CA and/or CA_2 bonding phases were completely or partially destroyed, depending on the degree of sulfidation, and CaS formed in all the tested castables. Large volume expansion was associated with the sulfidation of CaO due to the formation of the less dense compound CaS. It appears that sulfur corrosion is very similar to

alkali corrosion, i.e., both involve bonding phase attack and low density compound formation.

B. Gasifier Refractories

Coal gasification usually consists of a series of chemical reactions, i.e., combustion reactions, steam-carbon reactions, water-gas shift reactions, and methanation reactions. The operating temperature ranges are 870°C to 1040°C for the low temperature stage, and 1400°C to 1800°C for the high temperature stage. Pressure varies from ambient to 100 atmospheres. The gas atmosphere is composed of CO, CH_4, CO_2, H_2, and steam. The combination of the highly reducing gas mixture, steam, and corrosive impurities requires special considerations in selecting gasifier refractories. The influence of the gas atmosphere on the physical properties of various refractory castables has been extensively studied.[15-24]

It was found that silica was removed from refractory by H_2 reduction. But the reaction does not proceed when H_2 is wet. However, when large amounts of steam are present, as in coal gasification atmospheres, a completely different mechanism may be operative. In this case, steam dissolves and/or distills silica at a temperature as low as 815°C under pressure, and weakens the silica containing refractories by precipitating the silica in a cold area.[25] Therefore, the recommended refractories for coal gasifiers are dense alumina shapes or castables with low silica and iron contents on the hot face backed with bubble alumina insulating shape or insulating alumina castable with low silica and iron contents. The low silica requirement suggests that calcium aluminate cement be used as the bonding phase and tabular alumina as

the aggregate.

C. SOLGASMIX-PV Program

Numerous methods have been reported for calculating thermodynamic equilibrium compositions. All the techniques are based on the method of either Brinkley[26-27] or White et al.[28] Brinkley's method requires the determination of the equilibrium constants of all the possible reactions involved. A simpler method was suggested by White et al. using the direct minimization of the total free energy of the system. This technique was extended by Eriksson to include several condensed phases in the system, and a computer program SOLGAS was developed for performing the calculations.[29] The SOLGAS can only calculate equilibrium compositions in systems containing an ideal gas mixture and condensed phases of invariant stoichiometry. Later, Rosen and Eriksson expanded the method to also handle liquid and solid mixtures, as well as an ideal gas mixture.[30] However, immiscible melts or non-stoichiometric solids may occur in some cases. In order to handle condensed solutions as well as condensed solids with non-stoichiometric compositions, the SOLGAS was modified by Eriksson, and called SOLGASMIX.[31] The new SOLGASMIX enables the calculation of equilibrium compositions of systems containing a gas mixture, condensed solutions, and condensed phases of non-stoichiometry at constant pressure and variable temperatures. Non-ideal solutions can also be treated provided activity coefficients are available.

SOLGASMIX was later modified by Besmann using the ideal gas law and was called SOLGASMIX-PV.[32] SOLGASMIX-PV is capable of calculating equilibria at a constant total gas volume with variable total pressure.

As a result, the equilibrium compositions can be obtained at variable pressures and temperatures. This is an important feature in calculating the equilibrium alkali and/or alkali-sulfur species at different operating temperatures and pressures.

III. Principles of Calculations

The calculation of equilibrium compositions in a given system is based on the minimization of the total free energy under the constraint of mass conservation. Mathematically, this is equivalent to finding a minimum value of a curved surface subject to the constraint (or side condition) of mass balance. Lagrange's method appears to be most suitable in solving this kind of boundary conditions. Suppose f and g are functions of x, y, and z, and we wish to find the extrema of f (x, y, z) subject to the constraint of g (x, y, z) = 0. Then a new function W can be defined as a function of four variables,

$$W = f(x, y, z) + \lambda g(x, y, z)$$

where the variable is called Lagrange multiplier. The values of x, y, and z which give the extrema of f are among the simultaneous solutions of the following four equations in four unknowns,

$$W_x = 0,\ W_y = 0,\ W_z = 0,\ W_\lambda = g(x, y, z) = 0$$

where W_x, W_y, W_z, and W_λ represent the partial derivatives of W with respect to x, y, z, and λ.

When there are more than one constraint, e.g., finding the extrema of f (x, y, z) subject to two constraints,

$$g(x, y, z) = 0 \quad \text{and} \quad h(x, y, z) = 0,$$

the function W can be expressed as

$$W = f(x, y, z) + \lambda_1 g(x, y, z) + \lambda_2 h(x, y, z)$$

The values of x, y, and z which yield the extrema of f are then among the solutions of the following five equations in five unknowns:

$$W_x = 0,\ W_y = 0,\ W_z = 0,\ W_{\lambda 1} = 0,\ W_{\lambda 2} = 0$$

The number of unknowns and constraints can be extended, and the simultaneous equations, if linear, can be solved by the Gaussian elimination method.

Basic Equations

The total free energy G of a system can be expressed as

$$G = \sum_i x_i \, g_i$$

where x_i denotes the mole number of a species i, and g_i is the chemical potential defined as

$$g_i = g_i^o + RT \ln a_i$$

For the gaseous species, which are treated ideally, the activity a_i is equal to the partial pressure p_i,

$$a_i = p_i = (x_i/X) \, P$$

X and P denote the total number of moles in the gas phase and the total pressure respectively. For the condensed species, which are thought to be pure, the activity equals unity. Using the definitions above, a dimensionless quantity G/RT can be obtained,

$$G/RT = \sum_{i=1}^{m} x_i^g \left[(g^o/RT)_i^g + \ln P + \ln (x_i^g/X) \right] + \sum_{i=1}^{s} x_i^c \, (g^o/RT)_i^c . \qquad (1)$$

The indices g and c indicate the gas phase and the condensed phase, respectively. The number of species in the gas phase is denoted by m, and s is the number of condensed phases assumed to be present at equilibrium.

The mass balance constraint can be written as

$$\sum_{i=1}^{m} a_{ij}^g \, x_i^g + \sum_{i=1}^{s} a_{ij}^c \, x_i^c = b_j \quad (j = 1, 2, ----, \ell) \qquad (2)$$

or

$$\sum_{i=1}^{m} a_{ij}^{g} x_i^{g} + \sum_{i=1}^{s} a_{ij}^{c} x_i^{c} - b_j = 0 \quad (j = 1, 2, ----, \ell)$$

where a_{ij} represents the number of atoms of the j^{th} element of the i^{th} species; b_j is the total number of moles of the j^{th} element, and ℓ is the total number of elements. It should be noted that there are ℓ constraints in this case.

The problem now is to find the x_i's that give the minimum value of equation (1) subject to the constraints of equation (2). Once the x_i's are solved, the amount of the species present at equilibrium will be automatically determined.

According to Lagrange's method, W can be expressed as a combination of equations (1) and (2),

$$W = \sum_{i=1}^{m} x_i^{g} \left[(g^{o}/RT)_i^{g} + \ln P + \ln (x_i^{g}/X)\right] + \sum_{i=1}^{s} x_i^{c} (g^{o}/RT)_i^{c}$$

$$+ (\lambda_1 + \lambda_2 + ---- \lambda_\ell) \left(\sum_{i=1}^{m} a_{ij}^{g} x_i^{g} + \sum_{i=1}^{s} a_{ij}^{c} x_i^{c} - b_j\right) \qquad (3)$$

By taking the partial derivatives of W with respect to x_i^{g}, x_i^{c}, and λ_j equal to zero, the following equations are obtained (remembering that the partial derivative of G with respect to x_i is the chemical potential of species i):

$$(g^{o}/RT)_i^{g} + \ln P + \ln (x_i^{g}/X) - \sum_{j=i}^{\ell} \lambda_j a_{ij}^{g} = 0 \quad (i = 1, 2, ----, m) \qquad (4)$$

$$(g^{o}/RT)_i^{c} - \sum_{j=i}^{\ell} \lambda_j a_{ij}^{c} = 0 \quad (i = 1, 2, ----, s) \qquad (5)$$

and

$$\sum_{i=1}^{m} a_{ij}^{g} x_i^{g} + \sum_{i=1}^{s} a_{ij}^{c} x_i^{c} - b_j = 0 \quad (j = 1, 2, ----, \ell) \tag{6}$$

With $(m+s+\ell)$ equations, the $(m+s+\ell)$ unknowns can be solved. However, since there are non-linear terms involved and the Gaussian method is not applicable to non-linear equations, equation (4) and (6) are expanded in Taylor series about an arbitrary point $(y_1^g, y_2^g, \text{---} y_m^g, y_1^c, y_2^c, \text{---} y_s^c)$, neglecting terms involving second and higher order derivatives:

$$(g^o/RT)_i^g + \ln P + \ln (y_i^g/Y) - \sum_{j=1}^{\ell} \lambda_j a_{ij}^{g} + (x_i^g/y_i^g) - (X/Y) = 0$$
$$(i = 1, 2, ----, m) \tag{7}$$

$$\sum_{i=1}^{m} a_{ij}^{g} y_i^{g} + \sum_{i=1}^{s} a_{ij}^{c} y_i^{c} - b_j + \sum_{i=1}^{m} a_{ij}^{g} (x_i^{g} - y_i^{g}) + \sum_{i=1}^{s} a_{ij}^{c} (x_i^{c} - y_i^{c}) = 0$$
$$(j = 1, 2, ----, \ell) \tag{8}$$

where $Y = \sum_{i=1}^{m} y_i^{g}$ and $X = Y + x_i^{g} - y_i^{g}$.

Y_i's are the initial estimates of the moles in the equilibrium mixture. Improved values of y_i's are calculated (x_i's), which are used as a new guess for the next iteration cycle, and so on, until the equilibrium composition is obtained. Every iteration cycle will start with a new set of y_i values.

Equations (5), (7), and (8) constitute a set of $(m+s+\ell)$ linear equations with $(m+s+\ell)$ unknowns, and can be further simplified. From equation (7), x_i is calculated:

$$x_i^{g} = - f_i + y_i^{g} \left[(X/Y) + \sum_{j=1}^{\ell} \lambda_j a_{ij}^{g}\right] \quad (i = 1,2, ----, m) \tag{9}$$

where

$$f_i = y_i^g \left[(g^o/RT)_1^g + \ln P + \ln (y_i^g/Y) \right] \quad (i = 1, 2, ----, m)$$

The summation of equation (9) over i gives

$$\sum_{j=1}^{\ell} \lambda_j \sum_{i=1}^{m} y_i^g a_{ij}^g = \sum_{i=1}^{m} f_i \tag{10}$$

Substitution of equation (9) into equation (8) gives

$$\sum_{k=1}^{\ell} \lambda_k r_{jk} + [(X/Y)-1] \sum_{i=1}^{m} a_{ij}^g y_i^g + \sum_{i=1}^{s} a_{ij}^c x_i^c = \sum_{i=1}^{m} a_{ij}^g f_i -$$

$$\sum_{i=1}^{m} a_{ij}^g y_i^g + b_j \quad (j = 1, 2, ----, \ell) \tag{11}$$

where

$$r_{jk} = r_{kj} = \sum_{i=1}^{m} (a_{ij}^g a_{ik}^g) y_i^g \quad (j,k = 1, 2, ----, \ell)$$

Now equations (5), (10), and (11) constitute a set of (ℓ+s+1) linear equations with (ℓ+s+1) unknowns. The unknown quantities are λ_j (j = 1,2, ---,ℓ), x_i (i = 1,2, ---, s), and [(X/Y) - 1]. Notice that the solution gives directly the x_i^c values, while the x_i^g values are calculated by equation (9).

In order to avoid too many iterations, it is necessary to adopt a lowest y_i value. If the mole number of a species becomes less than the lowest value predetermined, y_i is set equal to zero, and then

that species will not be considered in the subsequent iterations.

It is obvious that the complexity is strongly dependent on the number of elements and condensed phases present in the system. The larger these numbers are, the more iteration cycles will be required to calculate the equilibrium compositions.

IV. Procedure

The calculation of equilibrium composition using SOLGASMIX-PV involves the following steps:

1. Define the thermodynamic system
2. Define the reference state
3. Input the thermodynamic data for each species in the system
4. Input the chemical formula for each species
5. Specify the total amount (in g-atom) of each element in the system.

A thermodynamic system may consist of a combination of gas species, liquid species, and solid species at the temperature and pressure considered. For all cases, the gas species are assumed to form an ideal gas mixture. The liquid species may form a single solution, or several solutions. The solid species can also form solid solutions or, for most cases, exist as stoichiometric compounds. The condensed solutions can be either ideal or non-ideal. A system defined this way will show the number of solutions and invariant phases possibly formed in the system, as well as the number of species in each solution.

The thermodynamic data required for the calculations are the Gibbs free energy of formation, ΔG_f. ΔG_f can be obtained by forming the compound from oxides or elements. In the present calculations, all the G_f's are based on the free energy of formation from the elemental states. Therefore, the reference state of each element in the system needs to be specified at each temperature, since ΔG_f is directly related to these reference states.

For the consideration of mass conservation, the constituent elements of each species, i.e., the chemical formula, and the total amount of each element are also required as input data. At equilibrium, the sum of a specific element from all the species containing it should be equal to the original amount of that element. The equilibrium composition is obtained by distributing all the elements in the system to achieve the minimum free energy.

Two series of calculations were carried out in studying the alkali and/or alkali-sulfur corrosion. The first one deals with the identification of the alkali and/or alkali-sulfur species existing in the coal gasification atmosphere. The second predicts the phases formed from the alkali-cement and alkali-sulfur-cement reactions. The thermodynamic data used for the calculations were compiled from various sources.[33-45]

A. Equilibrium Alkali and/or Alkali-Sulfur Species Calculations

In this series of calculations, the thermodynamic system contains one gas mixture, one liquid solution, and various invariant solid phases. The liquid solution is assumed to be ideal, and all the solid phases occur as stoichiometric compounds. The simulated coal gasification atmosphere is listed in Table 1. Since the operating conditions of the coal gasifier vary with different processes, calculations were performed at temperatures from 800 K to 1900 K and pressures from ambient to 100 atmosphere.[46] There are four cases related to this series of calculations, depending on the impurity present in the coal.

Table 1. Composition of Gas Atmosphere (in mol %)

H_2	CH_4	CO	CO_2	H_2O	N_2
12	18	17	12	20	20

1. Identification of Sodium Species

In this case, coal contains sodium species as a main impurity, and corrosion is due to the presence of the sodium species. The sodium content in this calculation is fixed at a level such that when all the sodium species vaporizes, the total sodium concentration in the gaseous phase is approximately 1 mol %. Table 2 shows all the sodium species for the thermodynamic system. Both the sodium species and the coal gasification atmosphere (Table 1) are included in the thermodynamic system.

2. Identification of Sodium-Sulfur Species

In this case, the coal contains both sodium and sulfur impurities, and corrosion is caused by both sodium and sulfur. The sodium content is fixed as described in case 1. The sulfur content is fixed at a level such that the concentration of H_2S in the gaseous phase is approximately 0.7 mol%. The species possibly present after sodium and sulfur are introduced to the coal gasification atmosphere are shown in Table 3.

3. Identification of Potassium Species

In this case, coal contains potassium as the main impurity, and corrosion results from the presence of the potassium impurity. The potassium content in the thermodynamic system is fixed in the same manner as the sodium content described in case 1, except sodium is replaced by potassium. The possible reactive potassium species generated in the coal gasification atmosphere are listed in Table 4.

Table 2. Sodium Species Considered in Calculations

Gas Mixture	Liquid Solution	Solid Phase
H_2, Na, CH_4, Na^+, CO, Na_2, CO_2, NaO, H_2O, NaO^-, NH_3, NaCN, O_2, NaOH, N_2	Na, Na_2O, NaOH, Na_2CO_3, NaCN	C, Na_2O_2, Na_2O, NaO_2, NaOH, Na_2CO_3, NaCN

Table 3. Sodium-Sulfur Species Considered in Calculations

Gas Mixture	Liquid Solution	Solid Phase
H_2, SO_2, CH_4,	Na, Na_2O, NaOH,	C, Na_2O_2, NaO_2,
CH_4, SO_3, CO,	Na_2CO_3, NaCN, H_2SO_4,	NaOH, Na_2CO_3, NaCN,
H_2SO_4, CO_2, NH_3,	H_4SO_5, H_6SO_6, H_8SO_7,	Na_2SO_4, Na_2S
H_2O, Na, Na_2SO_4,	$H_{10}SO_8$, Na_2SO_4, Na_2S	
Na^+, O_2, Na_2,		
N_2, NaO, S_2,		
NaO^-, CS_2, NaCN,		
COS, NaOH, H_2S		

Table 4. Potassium Species Considered in Calculations

Gas Mixture	Liquid Solution	Solid Phase
H_2, K, CH_4,	K, KOH, K_2CO_3,	C, K_2O_2, K_2O,
K^+, CO, K_2,	KCN	KOH, K_2CO_3, KCN
CO_2, KO, H_2O,		
KO^-, NH_3, KCN,		
O_2, KOH, N_2, K		

4. Identification of Potassium-Sulfur Species

In this case, coal contains both potassium and sulfur impurities, and corrosion is due to the presence of both potassium and sulfur. The potassium and sulfur contents were fixed at the same levels as described in case 2, i.e., approximately 1 mol% and 0.7 mol%, respectively, in the gaseous mixture. The possible reactive potassium-sulfur species in the coal gasification atmosphere are shown in Table 5. The thermodynamic data used in the above calculations are obtained from the JANAF tables.[33] The equilibrium compositions from the calculations will show the stable alkali and/or alkali-sulfur species existing in the coal gasification atmosphere at different temperatures and pressures. The reactive species obtained are then used to calculate the phases formed from the alkali-cement and/or alkali-sulfur-cement reactions.

B. Alkali-Cement and/or Alkali-Sulfur-Cement Reaction Calculations

The alkali corrosion, or the combined alkali-sulfur corrosion, is assumed to first start on the surface of the refractory lining. In order to simulate the corrosion process, only the surface layer was considered to participate in the reactions. The successive layers can be treated in the same manner as the surface layer. Therefore, in the simulated system, the amount of the cement tested was taken to be much less than the total gas quantity. This also insured against change in the composition of the gas phase upon reactions with the cement.

Both 53% and 72% alumina cements were tested in this series of calculations. The compositions of the cement are listed in Table 6. In addition to the coal gasification atmosphere (Table 1), the equilibrium

Table 5. Potassium-Sulfur Species Considered in Calculations

Gas Mixture	Liquid Solution	Solid Phase
H_2, K, CH_4,	K, KOH, KCN,	C, K_2O_2, K_2O,
K^+, CO, K_2,	K_2CO_3, H_2SO_4, H_4SO_5,	KOH, K_2CO_3, KCN,
CO_2, KO, H_2O,	H_6SO_6, H_8SO_7, $H_{10}SO_8$,	K_2SO_4, K_2S
KO^-, NH_3, KCN,	K_2SO_4, K_2S	
O_2, KOH, N_2,		
S_2, CS_2, COS,		
H_2S, SO_2, SO_3,		
H_2SO_4, K_2SO_4		

Table 6. Composition of Alumina Cement (in wt%)

	Al_2O_3	CaO	Fe_2O_3	SiO_2
Intermediate purity	53.5	40.5	1.6	4.4
High purity	71.5	27.9	0.17	0.16

alkali and/or alkali-sulfur species obtained from the previous calculations were also included in the testing atmosphere. Calculations were carried out at ambient pressure and temperatures from 900 K to 1800 K.

Each alumina cement was tested under four different atmospheres corresponding to the type of impurity present in the gasification atmosphere. Therefore, eight sets of results were obtained from this series of calculations. The results show the mineralogical change of the alumina cement under the influence of alkali and/or alkali-sulfur impurities.

V. Results and Discussion

A. Stable Alkali and/or Alkali-Sulfur Species

The stable alkali and/or alkali-sulfur species present in the coal gasification atmosphere can be identified at temperatures from 800 K to 1900 K and pressures from ambient to 100 atmosphere. Since there is a stable phase assemblage associated with each temperature and pressure, by changing the temperature and/or pressure, stable phase assemblages can be obtained throughout the temperature and pressure range considered. A boundary curve was formed by joining all the points that separate two stable phase regions. Finally, a P-T diagram was constructed for the multicomponent system.

1. P-T Diagram for Sodium Species

There are ten different phase regions for the stable sodium species as shown in Figure 1. At ambient pressure, the change of sodium species with temperature is as follows. At low temperatures, solid sodium carbonate is the stable sodium species. When temperature is increased, sodium carbonate melts at roughly 1130 K. Above 1270 K, sodium vapor begins to form by the reaction

$$Na_2CO_{3(s)} + 2C_{(s)} = 2Na_{(g)} + 3CO_{(g)}.$$

Above 1340 K, in addition to sodium vapor, sodium hydroxide vapor is generated by the reaction

$$Na_2CO_{3(s)} + H_2O_{(g)} + C_{(s)} = 2NaOH_{(g)} + 2CO_{(g)}.$$

Above 1400 K, sodium vapor and sodium hydroxide vapor are the only stable species. When pressure is increased above ambient pressure, some or all of the sodium and/or sodium hydroxide vapor will condense

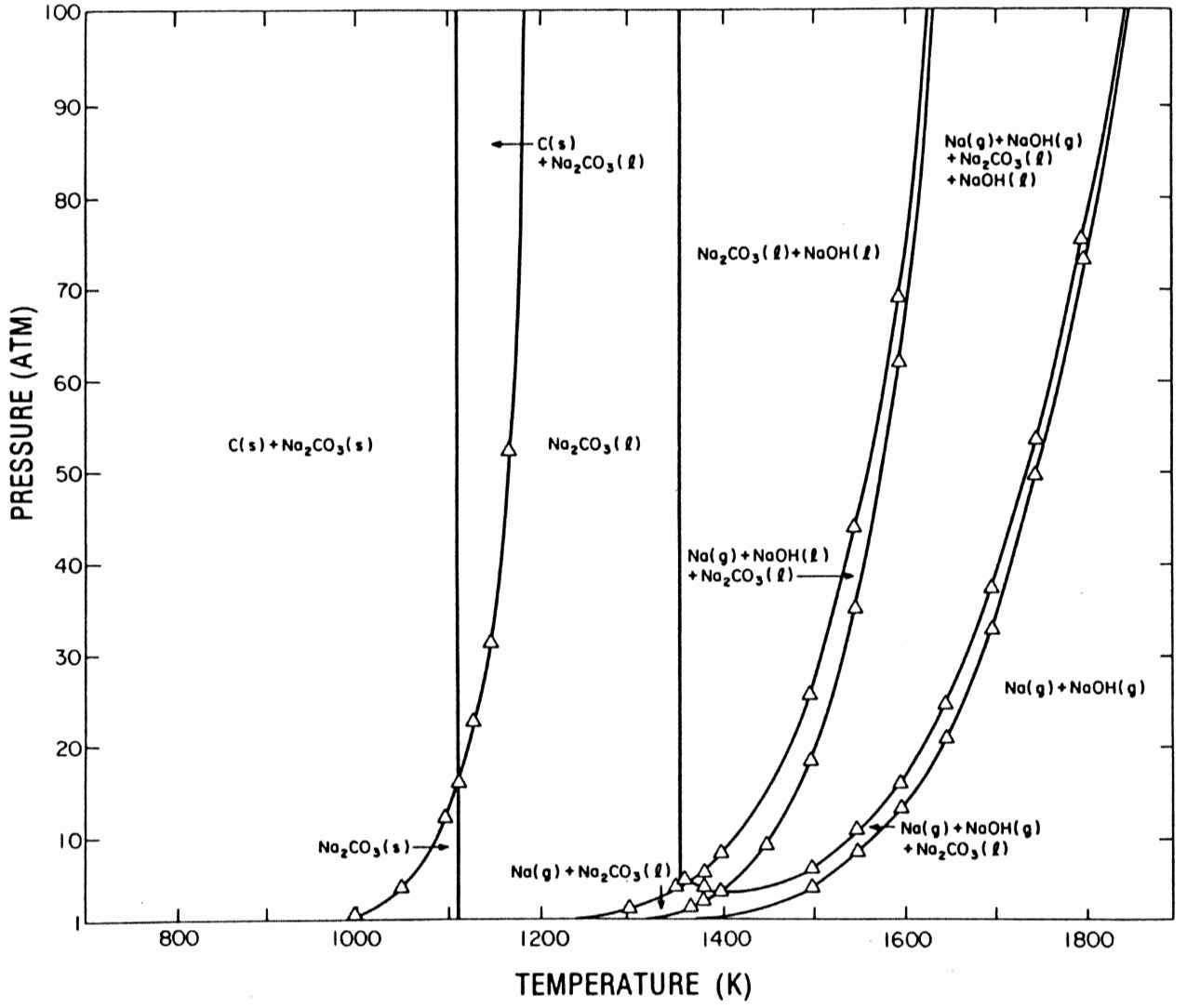

Figure 1. Stable sodium species in coal gasifier atmospheres.

to liquid as shown in the high pressure region of Figure 1. Also, carbon is deposited at low temperatures in the absence of an iron catalyst. The amount of deposited carbon increases with increasing pressure. Since high pressure favors the formation of CO_2, carbon is deposited by the reaction

$$2CO_{(g)} = CO_{2(g)} + C_{(s)}.$$

2. P-T Diagram for Sodium-Sulfur Species

The stable sulfur species in this case are H_2S gas and Na_2S in the form of solid or liquid. H_2S is present throughout the temperature and pressure range as shown in Figure 2. At ambient pressure, the change of the stable species with temperature is as follows. Below 975 K, all the sulfur impurities exist as H_2S and the sodium impurities as solid sodium carbonate. As temperature increases, sodium carbonate melts with the formation of both liquid and solid Na_2S. Above 1300 K, sodium vapor is generated, and sodium hydroxide vapor starts to form at 1450 K. No liquid exists above 1500 K, and the stable species are all vapor species, i.e., H_2S, Na vapor, and NaOH vapor. At medium high temperatures, sodium and/or sodium hydroxide vapor can be compressed to liquid by increasing pressure. However, when the temperature is sufficiently high, the presence of vapor species is independent of pressure. Increasing pressure can only condense part of the vapor species. Again, carbon deposition is found at low temperature and high pressure.

The presence of sulfur species tends to lower the liquidus temperature and increase the evaporation temperature of sodium species. When only sodium impurities are present, sodium carbonate melts at a temperature higher than 1100 K, while when sulfur impurities are added to the

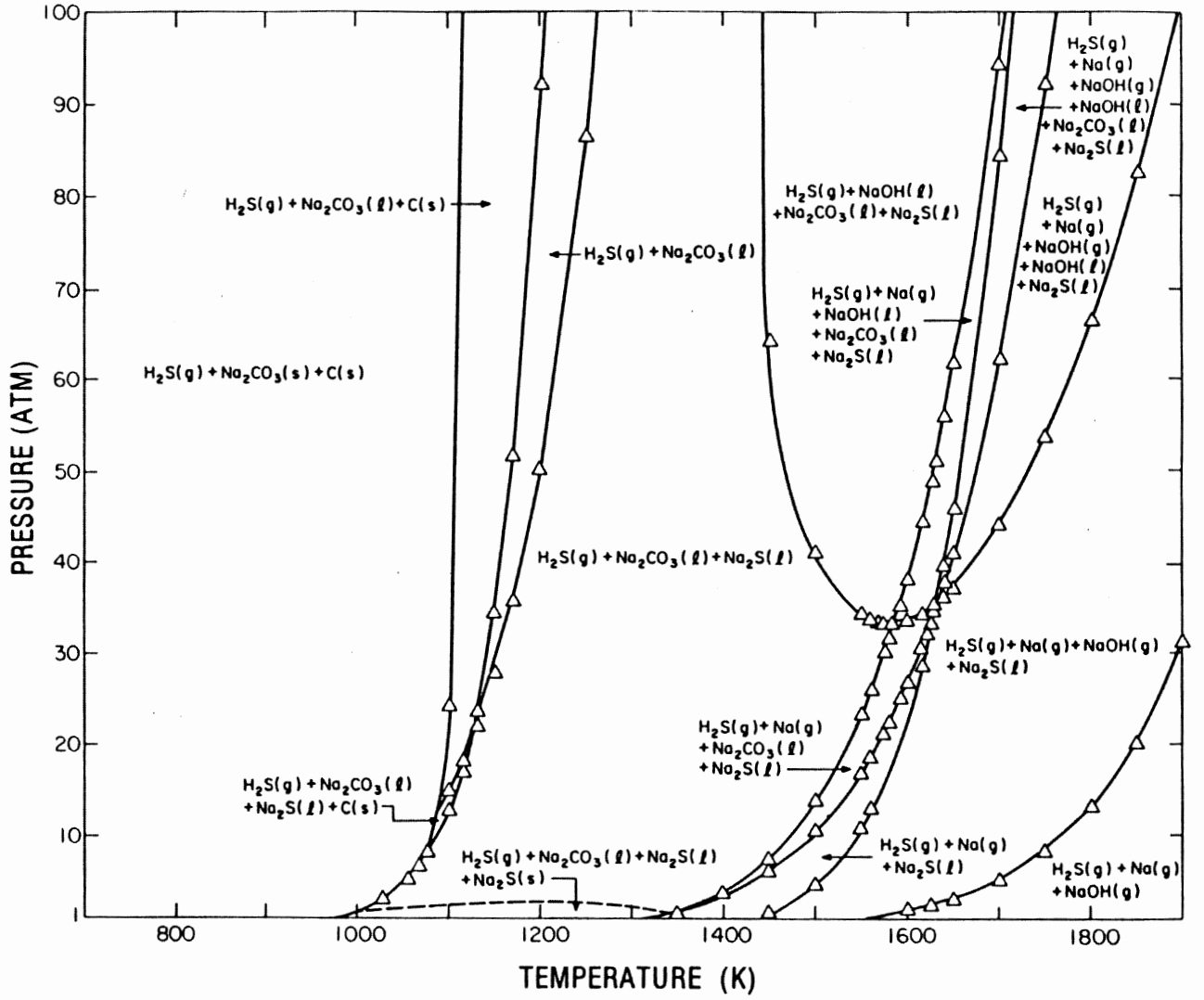

Figure 2. Stable sodium and sulfur species in coal gasifier atmospheres.

system, liquid starts to form around 1000 K. This can be explained by the Na_2CO_3 - Na_2S phase diagram shown in Figure 3.[47] The drop of liquid forming temperature is attributed to the eutectic point in the system.

3. P-T Diagram for Potassium Species

Similarities exist between the stable potassium species and sodium species. At ambient pressure, solid potassium carbonate is the stable form below 1170 K as shown in Figure 4. When temperature is increased, potassium carbonate melts at roughly 1170 K. Above 1200 K, potassium hydroxide vapor starts to form by the reaction

$$K_2CO_{3(s)} + H_2O_{(g)} + C_{(s)} = 2KOH_{(g)} + 2CO_{(g)}$$

Above 1250 K, in addition to potassium hydroxide vapor, potassium vapor is generated by the reaction

$$K_2CO_{3(s)} + 2C_{(s)} = 2K_{(g)} + 3CO_{(g)}$$

Above 1350 K, potassium and potassium hydroxide vapor are the only stable species present at ambient pressure. Carbon is also deposited at low temperature and high pressure. It should be noted that liquid potassium cyanide forms at high pressure, similar to cases reported for blast furnaces.[8] In general, potassium species are more volatile than sodium species, since the vapor potassium species occur at temperatures lower than the vaporization temperatures of sodium species.

4. P-T Diagram for Potassium-Sulfur Species

The stable sulfur species in this case are H_2S gas and solid or liquid K_2S in the gasification atmosphere. H_2S is present at all the temperatures and pressures considered as shown in Figure 5. At ambient pressure, the stable species change from solid phase to vapor phase as

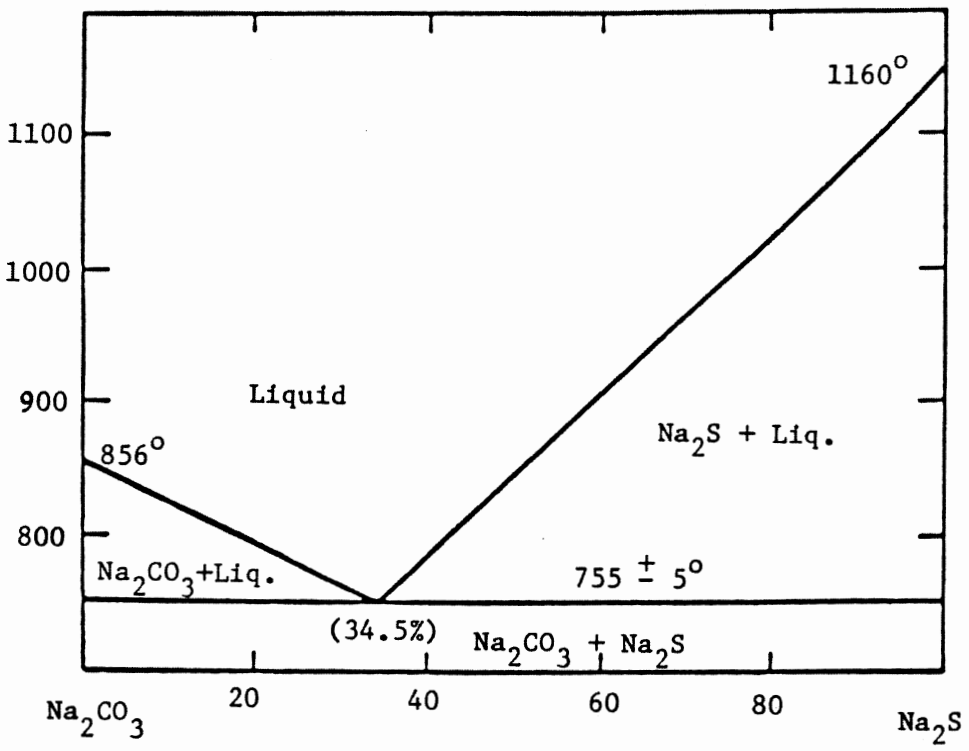

Figure 3. Na_2S-Na_2CO_3 phase diagram.

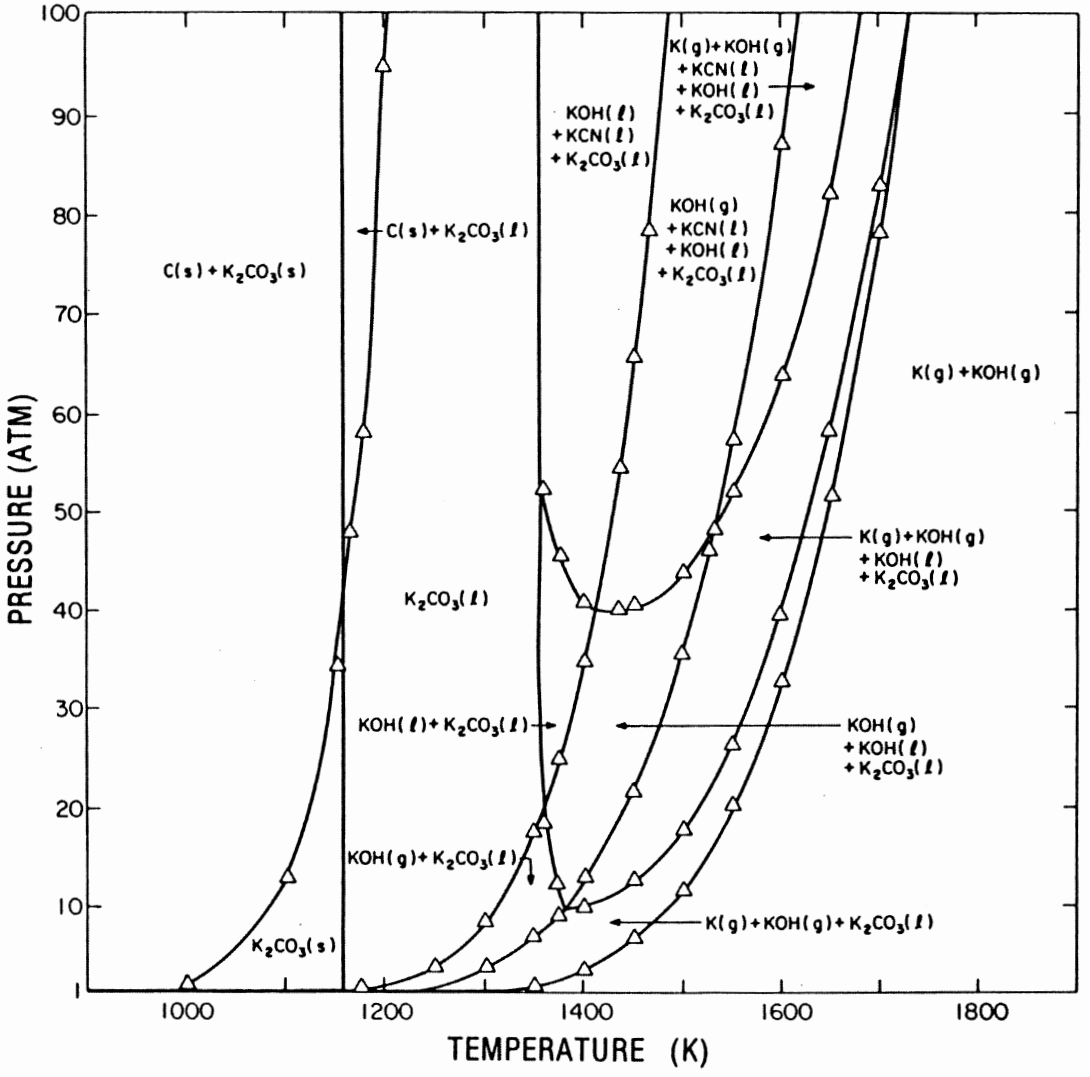

Figure 4. Stable potassium species in coal gasifier atmospheres.

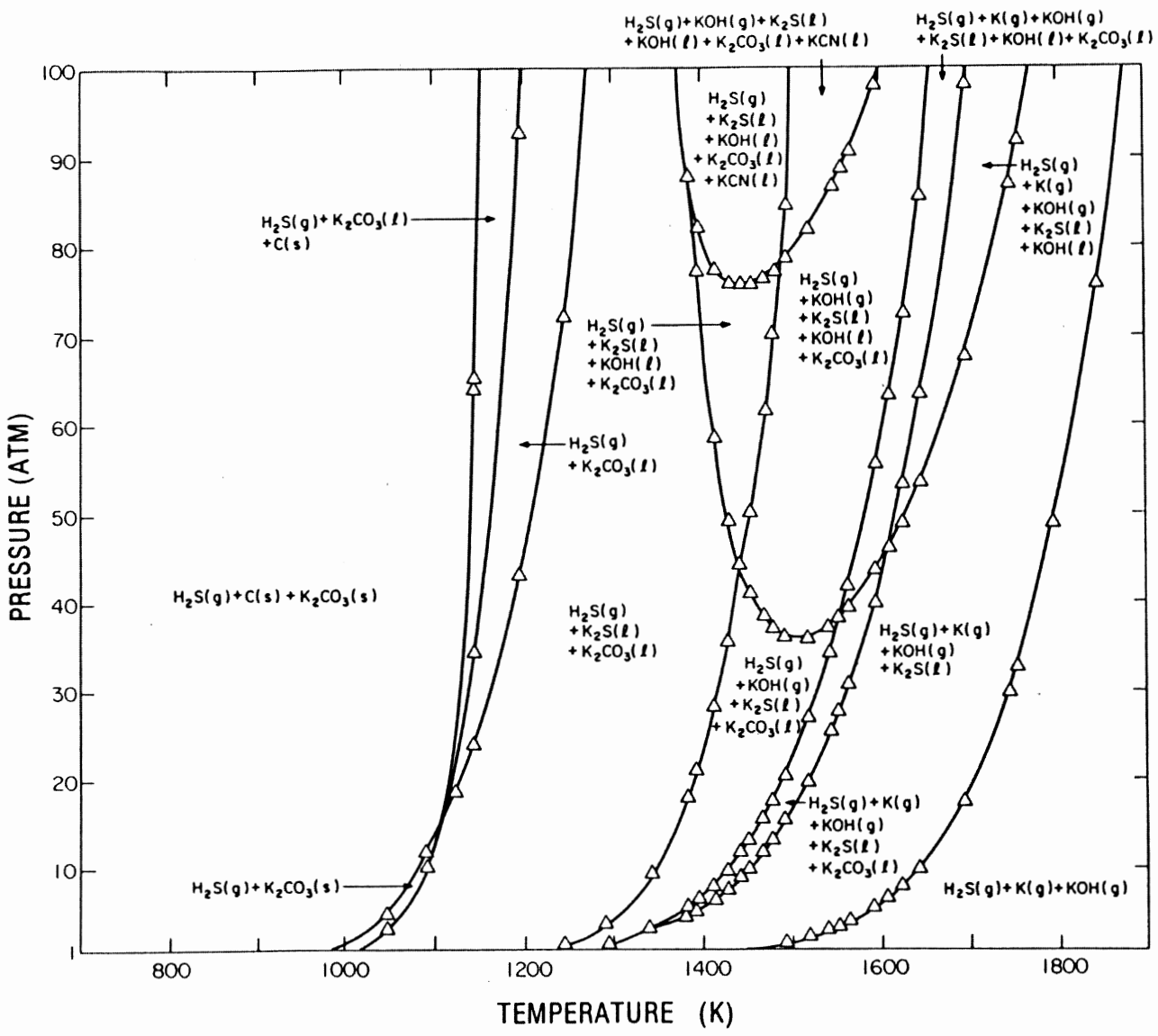

Figure 5. Stable potassium and sulfur species in coal gasifier atmospheres.

temperature is increased. Below 980 K, sulfur impurities occur as H_2S and potassium impurities as solid potassium carbonate. Above 1025 K, potassium carbonate melts to form a liquid of K_2CO_3 and K_2S. Above 1250 K, potassium hydroxide vapor adds to the stable phase assemblages. When the temperature is higher than 1300 K, potassium vapor is also generated. No liquid exists above 1465 K and the stable species are H_2S, potassium vapor, and potassium hydroxide vapor. Again, increasing the pressure can bring about partial or complete condensation of the vapor species, depending on the temperature.

The lowering of the liquid-forming temperature of the potassium species is also found. Although the K_2S - K_2CO_3 phase diagram is not available, similarities can be expected between the potassium and sodium system.

The P-T diagrams can be roughly divided into four regions, i.e., the solid phase region, the liquid phase region, the liquid and vapor phase region, and the vapor phase region; and the potentially reactive alkali and/or alkali-sulfur species can be identified in each region. As far as alkali attack is concerned, however, alkali vapor is the most undesirable species when compared with liquid or solid alkali species. Alkali vapors not only react with the gasifier lining, but circulate in the gasifier and extend the attacked area. Alkali circulation in the gasifier occurs by the following process:

Evaporation of alkali impurity to alkali vapor in the lower part (combustion zone) of the gasifier.

Transport of the alkali vapor by the gas stream generated from coal gasification.

Condensation of the alkali vapor to alkali liquid or alkali carbonate, depending on the temperature drop.

Re-evaporation of the alkali carbonate condensed on the charge when it reaches the lower part of the gasifier.

This circulation process can result in abnormally high alkali concentration in certain parts of the gasifier. For instance, under typical coal gasifier conditions in commercial-scale operations, a species with partial pressure as low as 10^{-6} atm would lead to vapor transport and deposition in metric ton quantities on an annual basis.[48] Alkali concentrations of 10 to 70 times higher than the average have been found in certain parts of the blast furnace.[9]

The state of alkali and/or alkali-sulfur species in contact with the refractory lining depends on the local temperature and pressure. If the temperature and pressure distribution in the gasifier are known, the cause and the type of reactions can be understood from the P-T diagram.

In the low temperature region, alkali corrosion is due to the presence of solid alkali carbonate. The reaction is either diffusion-controlled or interface-controlled. The corrosion problem in this region is considered relatively slow and less severe because the reactions involved are solid-state and sluggish. In the region where the temperature and pressure are such that liquid alkali is in contact with the refractory lining, corrosion may become serious. Apart from surface reactions, the alkali-liquid can infiltrate below the surface and form compounds there, generating internal stresses. In the region where alkali liquid and alkali vapor are in contact with the refractory lin-

ing, both liquid infiltration and vapor penetration may occur. In the region where temperature is the highest, the refractory lining is directly exposed to the alkali vapors. The corrosion problem may be threefold at this stage. Undesirable compound formation, direct surface fusion, and alkali circulation may occur. Refractories exposed to this temperature range will undergo the most serious attack.

It can be concluded that the extent of alkali attack depends on the alkali species participating in the reactions, which in turn depends on the temperature and pressure of the gasifier. Since alkali vapor is considered the most undesirable species, the alkali vapor should be excluded if possible or its concentration reduced to a minimum. The evaporation temperature of the alkali species increases with increasing pressure as shown in the P-T diagrams. As a result, by increasing the gasifier pressure, some or all of the alkali vapors will condense to liquid. The presence of sulfur impurities can decrease the alkali circulation since it increases the evaporation of the alkali species. However, the sulfur impurities can also react with the refractory lining, especially the calcium aluminate bonding phase, and are generally considered undesirable.

B. Reaction Products

When the active alkali and/or alkali-sulfur species are in contact with the refractory castables, chemical reactions occur as a result of reducing the total energy of the system. It is also known that the reactions primarily take place at the bonding phase. Using the alkali and/or alkali-sulfur species obtained above, phases formed from the

alkali-cement and/or alkali-sulfur-cement reactions can be predicted from the thermodynamic calculations. Two calcium aluminate cements, 53% and 72% alumina, were tested. The original phases present in the cements, determined by X-ray diffraction analyses, are shown in Table 7.

1. Exposure of 53% Alumina Cement to Alkali and/or Alkali-Sulfur Atmospheres

The 53% alumina cement was included in the four different atmospheres to calculate the equilibrium phases formed. Tables 8 through 11 show the mineralogical change of the 53% alumina cement at 1 atm after exposure to an atmosphere of sodium species, sodium-sulfur species, potassium species, and potassium-sulfur species, respectively. The difference between primary phase and secondary phase is the quantity of each phase formed. Secondary phases calculated are present in trace amounts, and may not be detected by X-ray diffraction analyses.

In the case of exposure to the sodium atmosphere, the primary phases formed are CaO and $Na_2O \cdot Al_2O_3$ at low temperatures. Above 1400 K, CaO disappeared with the formation of $3CaO \cdot Al_2O_3$. No sodium compound formed above 1600 K. In the case of exposure to the sodium-sulfur atmosphere, the primary phases formed are CaS, CaO, Na_2S, and $Na_2O \cdot Al_2O_3$ at low temperatures. Above 1300 K, CaO disappeared with the increased formation of CaS. No sodium compound formed above 1600 K, while CaS existed at all the testing temperatures. In the case of exposure to the potassium atmosphere, the primary phases formed are CaO and $K_2O \cdot Al_2O_3$ throughout the testing temperatures. In the case of exposure to the potassium-sulfur atmosphere, the primary phases formed are CaS, CaO, K_2S, and $K_2O \cdot Al_2O_3$ at low temperatures. Above 1100 K, CaO

Table 7. Mineralogical Composition of Cement

	Primary Phase	Secondary Phase
53% Alumina Cement	CA	C_2AS
72% Alumina Cement	CA	CA_2

$C = CaO$, $A = Al_2O_3$, $S = SiO_2$

Table 8. Phases Predicted for Sodium-53% Alumina Cement Reactions at 1 atm

Temperature	Primary Phases	Secondary Phases
1200 K	CaO, $Na_2O \cdot Al_2O_3$	Fe, NaOH, $Na_2O \cdot SiO_2$
1300 K	CaO, $Na_2O \cdot Al_2O_3$	Fe, $Na_2O \cdot SiO_2$
1400 K	CaO, $Na_2O \cdot Al_2O_3$	Fe, $2CaO \cdot SiO_2$
1500 K	$3CaO \cdot Al_2O_3$, $Na_2O \cdot Al_2O_3$	Fe, $2CaO \cdot SiO_2$
1600 K	$CaO \cdot Al_2O_3$, $3CaO \cdot Al_2O_3$	Fe, $2CaO \cdot SiO_2$
1700 K	$CaO \cdot Al_2O_3$, $3CaO \cdot Al_2O_3$	Fe, $2CaO \cdot SiO_2$
1800 K	$CaO \cdot Al_2O_3$, $3CaO \cdot Al_2O_3$	Fe, $2CaO \cdot SiO_2$

Table 9. Phases Predicted for Sodium-Sulfur-53% Alumina Cement Reactions at 1 atm

Temperature	Primary Phases	Secondary Phases
900 K	CaS, $CaCO_3$, Na_2S, $Na_2O \cdot Al_2O_3$	C, FeS, $Na_2O \cdot SiO_2$
1000 K	CaS, CaO, Na_2S, $Na_2O \cdot Al_2O_3O$	Fe, $Na_2O \cdot SiO_2$
1100 K	CaS, CaO, Na_2S, $Na_2O \cdot Al_2O_3$	Fe, $2CaO \cdot SiO_2$
1200 K	CaS, CaO, Na_2S, $Na_2O \cdot Al_2O_3$	Fe, $2CaO \cdot SiO_2$
1300 K	CaS, CaO, Na_2S, $Na_2O \cdot Al_2O_3$	Fe, $2CaO \cdot SiO_2$
1400 K	CaS, Na_2S, $Na_2O \cdot Al_2O_3$	Fe, $2CaO \cdot SiO_2$
1500 K	CaS, $Na_2O \cdot Al_2O_3$	Fe, $2CaO \cdot SiO_2$
1600 K	CaS, CaO Al_2O_3, $Na_2O \cdot Al_2O_3$	Fe, $2CaO \cdot SiO_2$
1700 K	CaS, $CaO \cdot Al_2O_3$	Fe, $2CaO \cdot SiO_2$
1800 K	CaS, $CaO \cdot Al_2O_3$	Fe, $2CaO \cdot SiO_2$

Table 10. Phases Predicted for Potassium-53% Alumina Cement Reactions at 1 atm

Temperature	Primary Phases	Secondary Phases
900 K	$CaCO_3$, $K_2O \cdot Al_2O_3$	Fe, C, KOH, K_2O, SiO_2
1000 K	CaO, $K_2O \cdot Al_2O_3$	Fe, KOH, $K_2O \cdot SiO_2$
1100 K	CaO, $K_2O \cdot Al_2O_3$	Fe, $K_2O \cdot SiO_2$
1200 K	CaO, $K_2O \cdot Al_2O_3$	Fe, $2CaO \cdot SiO_2$, $K_2O \cdot SiO_2$
1300 K	CaO, $K_2O \cdot Al_2O_3$	Fe, $2CaO \cdot SiO_2$
1400 K	CaO, $K_2O \cdot Al_2O_3$	Fe, $2CaO \cdot SiO_2$
1500 K	CaO, $K_2O \cdot Al_2O_3$	Fe, $2CaO \cdot SiO_2$
1600 K	CaO, $K_2O \cdot Al_2O_3$	Fe, $2CaO \cdot SiO_2$
1700 K	CaO, $K_2O \cdot Al_2O_3$	Fe, $2CaO \cdot SiO_2$
1800 K	CaO, $K_2O \cdot Al_2O_3$	Fe, $2CaO \cdot Al_2O_3 \cdot SiO_2$

Table 11. Phases Predicted for Potassium-Sulfur-53% Alumina Cement Reactions at 1 atm

Temperature	Primary Phases	Secondary Phases
900 K	CaS, $CaCO_3$, K_2S, $K_2O \cdot Al_2O_3$	C, $2CaO \cdot SiO_2$, FeS
1000 K	CaS, CaO, K_2S, $K_2O \cdot Al_2O_3$	Fe, $2CaO \cdot SiO_2$
1100 K	CaS, CaO, K_2S, $K_2O \cdot Al_2O_3$	Fe, $2CaO \cdot SiO_2$
1200 K	CaS, K_2S, $K_2O \cdot Al_2O_3$	Fe, $2CaO \cdot SiO_2$
1300 K	CaS, K_2S, $K_2O \cdot Al_2O_3$	Fe, $2CaO \cdot SiO_2$
1400 K	CaS, $K_2O \cdot Al_2O_3$	Fe, $2CaO\ SiO_2$, $K_2O \cdot SiO_2$
1500 K	CaS, $K_2O \cdot Al_2O_3$	Fe, $2CaO \cdot SiO_2$
1600 K	CaS, $K_2O \cdot Al_2O_3$	Fe, $2CaO \cdot SiO_2$
1700 K	CaS, $K_2O \cdot Al_2O_3$	Fe, $2CaO \cdot SiO_2$
1800 K	CaS, $K_2O \cdot Al_2O_3$	Fe, $2CaO \cdot Al_2O_3 \cdot SiO_2$

disappeared with increased formation of CaS. Above 1300 K, the primary phases are CaS and $K_2O \cdot Al_2O_3$.

When sulfur impurities are not present, alkali impurities attack the bonding phase by the reaction

$$CaO \cdot Al_2O_3 + 2Na + 1/2O_2 = Na_2O \cdot Al_2O_3 + CaO$$

or

$$CaO \cdot Al_2O_3 + 2K + 1/2O_2 = K_2O \cdot Al_2O_3 + CaO$$

For simplicity, Na and K are used to represent the reacting alkali species. The actual alkali species can be alkali carbonate, alkali liquid, or alkali vapors, depending on the P-T diagrams. It should be noted that free lime is released when sodium aluminate or potassium aluminate is formed. In a steam-rich atmosphere, the free lime may pick up water and cause the refractory lining to "perish." In the exposure to the potassium atmosphere, lime and potassium aluminate are present at all the testing temperatures. However, anomalies were found in the calculations of the sodium reactions because lime and sodium aluminate become unstable above 1400 K and 1600 K, respectively. The anomalies are attributed to the accuracy of the thermodynamic data of sodium aluminate. When the formation energy of sodium aluminate was made close to that of potassium aluminate, the anomalies disappeared. That is, lime and sodium aluminate become stable, and $3CaO \cdot Al_2O_3$ becomes unstable.

When sulfur impurities are present, the CaO released from the alkali-cement reactions is sulfidized by the reaction

$$CaO + H_2S = CaS + H_2O$$

or

$$CaO + Na_2S = CaS + 2Na + 1/2O_2$$

Again, anomalies were found in the calculations when sodium aluminate was present. The sulfidation can also occur directly on the bonding phase according to the reaction

$$CaO \cdot Al_2O_3 + H_2S = CaS + Al_2O_3 + H_2O$$

The released alumina is then reacted with the sodium or potassium species to form sodium aluminate or potassium aluminate.

2. Exposure of 72% Alumina Cement to Alkali and/or Alkali-Sulfur Atmosphere

Similar results are obtained for the 72% alumina cement reactions. The equilibrium phases predicted from calculations under the sodium, sodium-sulphur, potassium, and potassium-sulfur atmospheres are shown in Tables 12 through 15.

In the exposure to the sodium atmosphere, the primary phases are CaO and $Na_2O \cdot Al_2O_3$ at low temperatures. Above 1400 K, CaO disappeared with the formation of $3CaO \cdot Al_2O_3$ and $CaO \cdot Al_2O_3$. No sodium compound formed above 1600 K. Above 1600 K, anomalies appeared. In the exposure to the potassium atmosphere, the primary phases formed are CaO and $K_2O \cdot Al_2O_3$ throughout the temperature range. In the exposure to the potassium atmosphere, the primary phases formed at all the testing temperatures.

Again, the major reactions in forming alkali aluminate and releasing lime are

$$CaO \cdot Al_2O_3 + 2Na + 1/2O_2 = Na_2O \cdot Al_2O_3 + CaO$$

and

$$CaO \cdot Al_2O_3 + 2K + 1/2O_2 = K_2O \cdot Al_2O_3 + CaO$$

Sulfidation also occurred by

Table 12. Phases Predicted for Sodium-72% Alumina Cement Reactions at 1 atm

Temperature	Primary Phases	Secondary Phases
1200 K	CaO, $Na_2O \cdot Al_2O_3$	Fe, $Na_2O \cdot SiO_2$
1300 K	CaO, $Na_2O \cdot Al_2O_3$	Fe, $Na_2O \cdot SiO_2$
1400 K	CaO, $Na_2O \cdot Al_2O_3$	Fe, $2CaO \cdot SiO_2$
1500 K	$3CaO \cdot Al_2O_3$, $CaO \cdot Al_2O_3$, $Na_2O \cdot Al_2O_3$	Fe, $2CaO \cdot SiO_2$
1600 K	$CaO \cdot Al_2O_3$, $Na_2O \cdot Al_2O_3$	Fe, $2CaO \cdot SiO_2$
1700 K	$CaO \cdot Al_2O_3$, $CaO \cdot 2Al_2O_3$	Fe, $2CaO \cdot SiO_2$
1800 K	Al_2O_3, $CaO \cdot Al_2O_3$	Fe, $2CaO \cdot Al_2O_3 \cdot SiO_2$

Table 13. Phases Predicted for Sodium-Sulfur-72% Alumina Cement Reactions at 1 atm

Temperature	Primary Phases	Secondary Phase
900 K	CaS, Na_2S, $Na_2O \cdot Al_2O_3$	C, FeS, $Na_2O \cdot SiO_2$
1000 K	CaS, Na_2S, $Na_2O \cdot Al_2O_3$	FeS, $Na_2O \cdot SiO_2$
1100 K	CaS, Na_2S, $Na_2O \cdot Al_2O_3$	FeS, $Na_2O \cdot SiO_2$
1200 K	CaS, Na_2S, $Na_2O \cdot Al_2O_3$	Fe, $Na_2O \cdot SiO_2$
1300 K	CaS, Na_2S, $Na_2O \cdot Al_2O_3$	Fe, $2CaO \cdot SiO_2$
1400 K	CaS, Na_2S, $Na_2O \cdot Al_2O_3$	Fe, $2CaO \cdot SiO_2$
1500 K	CaS, $Na_2O \cdot Al_2O_3$	Fe, $2CaO \cdot SiO_2$
1600 K	CaS, $CaO \cdot Al_2O_3$, $Na_2O \cdot Al_2O_3$	Fe, $2CaO\ Al_2O_3 \cdot SiO_2$
1700 K	$CaO \cdot Al_2O_3$, $CaO \cdot 2Al_2O_3$	Fe, $2CaO \cdot Al_2O_3 \cdot SiO_2$
1800 K	Al_2O_3, $CaO \cdot Al_2O_3$	Fe, $2CaO \cdot Al_2O_3 \cdot SiO_2$

Table 14. Phases Predicted for Potassium-72% Alumina Cement Reactions at 1 atm

Temperature	Primary Phases	Secondary Phases
900 K	$CaCO_3$, $K_2O \cdot Al_2O_3$	C, Fe, KOH, $K_2O \cdot SiO_2$
1000 K	CaO, $K_2O \cdot Al_2O_3$	Fe, KOH, $K_2O \cdot SiO_2$
1100 K	CaO, $K_2O \cdot Al_2O_3$	Fe, $K_2O \cdot SiO_2$
1200 K	CaO, $K_2O \cdot Al_2O_3$	Fe, $K_2O \cdot SiO_2$
1300 K	CaO, $K_2O \cdot Al_2O_3$	Fe, $2CaO \cdot SiO_2$
1400 K	CaO, $K_2O \cdot Al_2O_3$	Fe, $2CaO \cdot SiO_2$
1500 K	CaO, $K_2O \cdot Al_2O_3$	Fe, $2CaO \cdot SiO_2$
1600 K	CaO, $K_2O \cdot Al_2O_3$	Fe, $2CaO \cdot SiO_2$
1700 K	CaO, $K_2O \cdot Al_2O_3$	Fe, $2CaO \cdot SiO_2$
1800 K	CaO, $CaO \cdot Al_2O_3$, $K_2O \cdot Al_2O_3$	Fe, $2CaO \cdot Al_2O_3 \cdot SiO_2$

Table 15. Phases Predicted for Potassium-Sulfur-72% Alumina Cement Reactions at 1 atm

Temperature	Primary Phase	Secondary Phase
900 K	CaS, K_2S, $K_2O \cdot Al_2O_3$	C, FeS, $K_2O \cdot SiO_2$
1000 K	CaS, K_2S, $K_2O \cdot Al_2O_3$	FeS, $K_2O \cdot SiO_2$
1100 K	CaS, K_2S, $K_2O \cdot Al_2O_3$	FeS, $2CaO \cdot SiO_2$
1200 K	CaS, K_2S, $K_2O \cdot Al_2O_3$	Fe, $K_2O \cdot SiO_2$
1300 K	CaS, K_2S, $K_2O \cdot Al_2O_3$	Fe, $2CaO \cdot SiO_2$
1400 K	CaS, $K_2O \cdot Al_2O_3$	Fe, $2CaO \cdot SiO_2$
1500 K	CaS, $K_2O \cdot Al_2O_3$	Fe, $2CaO \cdot SiO_2$
1600 K	CaS, $K_2O \cdot Al_2O_3$	Fe, $2CaO \cdot SiO_2$
1700 K	CaS, $K_2O \cdot Al_2O_3$	Fe, $2CaO \cdot SiO_2$
1800 K	CaS, $K_2O \cdot Al_2O_3$	Fe, $2CaO \cdot Al_2O_3 \cdot SiO_2$

$$CaO + 1/2S_2 = CaS + 1/2O_2$$

or

$$CaO \cdot Al_2O_3 + 1/2S_2 = CaS + Al_2O_3 + 1/2O_2$$

The above results can be checked with the phase diagram. When only sodium or potassium species are present in the system, the phase diagrams used are Na_2O-Al_2O_3-CaO and K_2O-Al_2O_3-CaO. The composition corresponding to the present calculations of both 53% and 72% alumina cements are labeled in Figures 6 and 7, respectively. The original diagrams are shown by the solid line. Since it is unlikely to form compounds in the CaO-Na_2O and CaO-K_2O systems, and no compounds are found in the Na_2O-Na_2O Al_2O_3 systems, it is reasonable to approximate the diagrams as shown in Figures 6 and 7. The stable phase assemblage corresponding to the labeled composition is likely to consist of CaO and $Na_2O \cdot Al_2O_3$ for Figure 6, and CaO and $K_2O \cdot Al_2O_3$ for Figure 7. The third phase may exist either as alkali liquid or alkali vapor, depending on the temperature. When sulfur species as well as alkali species are present in the system, the reactions may proceed in two ways. If the alkali reactions occur first and sulfidation second, the lime from Figures 6 and 7 is then reacted with the sulfur species to form CaS with excess sulfur existing in the gas state. If sulfidation occurs first and alkali reaction second, after forming CaS, the system is reduced to the alkali-alumina system, i.e., Na_2O-Al_2O_3, or K_2O-Al_2O, and alkali aluminate will be formed with excess alkali existing in gas or liquid states or combined with the excess sulfur.

The alkali sulfide (Na_2S or K_2S) obtained from the calculations may give the impression that it can decrease the alkali and sulfur concen-

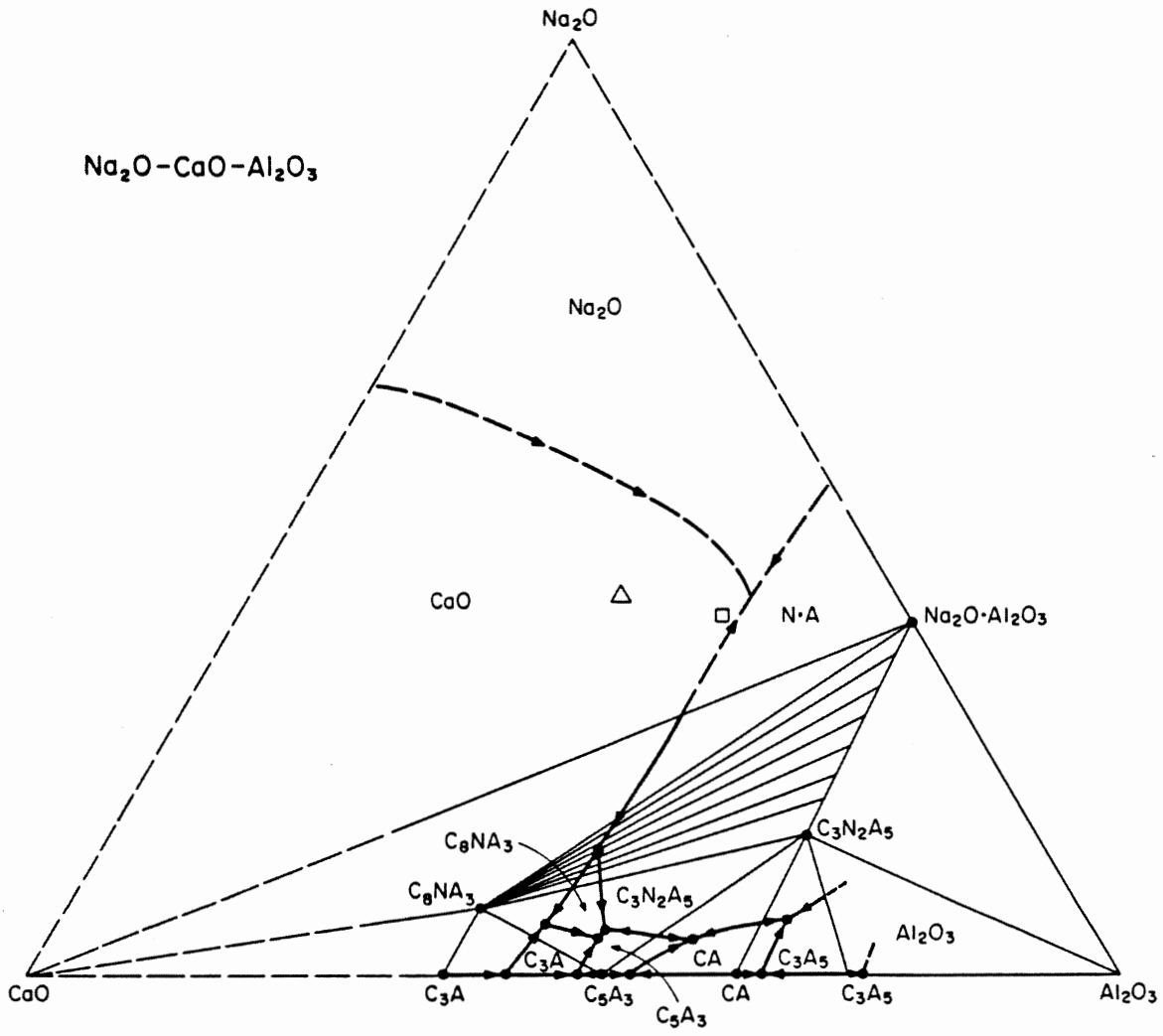

Figure 6. Na_2O-CaO-Al_2O_3 system. (△ and □ represent compositions used in calculations for 53% and 72% alumina cement, respectively.)

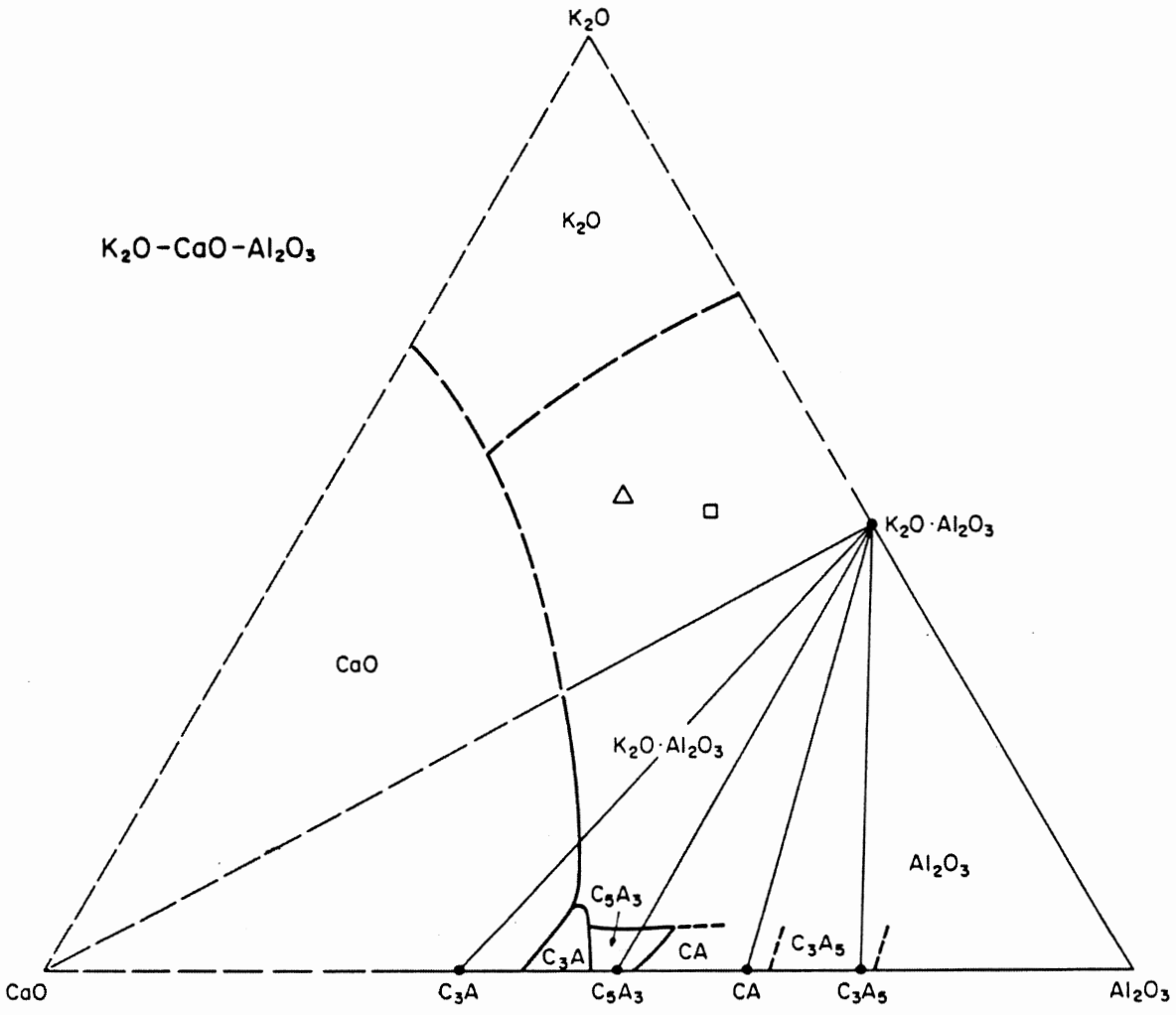

Figure 7. K_2O-CaO-Al_2O_3 system. (△ and □ represent compositions used in calculations for 53% and 72% alumina cement, respectively.)

trations, and therefore, reduce the alkali and/or alkali-sulfur attack. However, it was found that alkali sulfide exists only when excess alkali and sulfur are present after the alkali and sulfidation reaction. If the amount of alkali and sulfur are not sufficient to completely decompose calcium aluminate, alkali sulfide will not form. The phases formed are calcium sulfide, alkali aluminate, and residual calcium aluminate. As a result, adding excess sulfur or alkali to the alkali-containing system will not counteract the alkali or sulfidation reactions from the thermodynamic consideration.

Results from experiments also show agreements with the alkali-cement reactions. Both 53% and 72% alumina cement were mixed with sodium carbonate and potassium carbonate respectively in approximately 1:1 weight ratio as used in the calculations. The mixed samples were fired in the coal gasification atmosphere (Table 1). X-ray analyses of the reacted samples show the presence of CaO and $Na_2O \cdot Al_2O_3$ for the sodium reactions, and CaO and $K_2O \cdot Al_2O_3$ for the potassium reactions. At higher temperatures, results from experiments and calculations begin to deviate. This is probably due to the loss of sodium in the open system, resulting in an experimental gas composition different from that used in the calculations.

The important consequence of the above reactions is that compounds of lower densities are formed. The theoretical volume expansions associated with these reactions can be calculated provided the specific gravities of reactants and products are known. Table 16 lists the specific gravities used in calculating the volume expansions of the sodium-cement and sodium-sulfur-cement reactions.

Table 16. Specific Gravities used in Volume Expansion Calculations

CaO	Al_2O_3	CaS	$CaO \cdot Al_2O_3$
3.315	3.97	2.5	2.98

The volume expansions associated with the reactions

$$CaO \cdot Al_2O_3 + 2Na + 1/2\ O_2 = Na_2O \cdot Al_2O_3 + CaO$$

and

$$CaO \cdot Al_2O_3 + 2Na + 1/2\ S_2 = CaS + Na_2O \cdot Al_2O_3$$

are 46.7% and 69%, respectively.

VI. Conclusions

The mechanism of alkali and/or alkali-sulfur attack on coal gasifier lining consists of two steps: 1) the release of the alkali and/or alkali-sulfur species from coal, and 2) the reactions with the gasifier lining. The alkali and/or alkali-sulfur species present in the coal gasification atmosphere can be predicted from thermodynamic calculations. The alkali and sulfur compounds formed from the reactions can also be calculated. Results strongly depend on the accuracy of the thermodynamic data, especially when handling a system of more than 50 species.

The alkali and/or alkali-sulfur attack can result in:

1. Incipient melting of the hot face due to alkali fluxing
2. Thermal spalling due to differential thermal expansion of the bulk and the surface compounds
3. Traverse cracking due to internal stresses generated under the surface
4. Surface washout by dissolution of alkali compounds.

When refractories made from the Al_2O_3-SiO_2-CaO system are exposed to alkali atmospheres, alkali reactions appear to be an inevitable consequence from the viewpoint of thermodynamic considerations. Since the total energy of the system will be lowered by the formation of alkali compounds, the compounds formed are usually far less dense than the bulk. The attack can only be retarded by slowing the rate of the reactions. The recommended methods for retarding alkali attack are:

1. Elevate pressures rather than temperatures in operating conditions
2. Improve the reactor cooling system
3. Minimize the refractory porosity
4. Maximize the maturity of the bonding phase to develop a strong ceramic bond (this can be done by pre-firing the gasifier for several hundred hours without the presence of alkali).

The last point is especially important in that the aggregates remain unreacted to alkali impurity. This is attributed to the larger grain size and smaller surface area of the aggregates when compared to the cement bonding phase. Therefore, with improved bonding phases, the gasifier lining can be expected to last longer.

VII. References

1. J. W. Hastie, "High Temperature Vapors-Science and Technology," Academic Press: New York, NY, 1975.

2. R. L. Hirsch, J. E. Gallagher, Jr., R. R. Lessard, and R. D. Wesselhoft, "Catalytic Coal Gasification: An Emerging Technology," Science, Vol. 215, 1982, p. 121.

3. J. B. Tak and D. J. Young, "Sulfur Corrosion of Calcium Aluminate Bonded Castables," Am. Ceram. Soc. Bull., Vol. 61, No. 7, 1982, p. 725.

4. G. R. Rigby and R. Hutton, "Action of Alkali and Alkali-Vanadium Oxide Slags on Alumina-Silica Refractories," J. Am. Ceram. Soc., Vol. 45, No. 2, 1962, p. 68.

5. R. E. Farris and J. E. Allen, "Aluminous Refractories-Alkali Reactions," Iron and Steel Engineer, Feb., 1973, p. 67.

6. C. R. Kennedy, "Alkali Attack on a Mullite Refractory in the Grand Forks Energy Technology Center Slagging Gasifier," J. Materials for Energy Systems, Vol. 3, June, 1981, p. 27.

7. J. T. Shapland and A. F. Lirovich, "Evaluation of Five Commercial Calcium-Aluminate Cements," Am. Ceram. Soc. Bull., Vol. 43, No. 7, 1964, p. 510.

8. S. E. McCune, T. P. Greaney, W. C. Allen, and R. B. Snow, "Reaction Between K_2O and Al_2O_3-SiO_2 Refractories as Related to Blast-Furnace Linings," J. Am. Ceram. Soc., Vol. 40, No. 6, June 1957, p. 187.

9. P. H. Havranek, "Alkali Attack on Blast Furnace Refractories," Trans J. Brit. Ceram. Soc., Vol. 77, 1978, p. 92.

10. H. Insley, "Some Observations of Surface Deposits Formed on Glass-Furnace Regenerators," J. Am. Ceram. Soc., Vol. 9, No. 10, 1926, p. 635.

11. C. L. Thompson and E. P. Rexford, "Study of Alumina-Silica Checker-Brick from Regenerator of a Glass Tank," J. Am. Ceram. Soc., Vol. 21, No. 2, 1938, p. 55.

12. E. C. Petrie and D. P. Brown, "Observations on the Shelling of Checker-Brick," J. Am. Ceram. Soc., Vol. 31, No. 1, 1948, p. 14.

13. C. K. Jones and R. L. Hardy, "Petroleum Ash Components and Their Effect on Refractories," Industrial and Engineering Chemistry, Vol. 44, No. 11, Nov., 1952, p. 2615.

14. L. G. Huggett, "The Oil-Ash Problem," Trans. J. Brit. Ceram. Soc., Vol. 80, No. 1, 1981, p. 11.

15. D. W. Lang and D. E. Day, "Properties of High Alumina Refractories After Exposure to Steam/H_2 Atmospheres," Am. Ceram. Soc. Bull., Vol. 61, No. 4, 1982, p. 475.

16. D. E. Day, "Reaction of Alumina Ceramics with Saturated Steam," Am. Ceram. Soc. Bull., Vol. 62, No. 6, 1982, p. 624.

17. S. F. Rahman and D. E. Day, "Properties of Refractories After Exposure to High Pressure Gases: I-Survey of Commercial Products," J. Materials Energy Systems, Vol. 1, Dec. 1979, p. 34.

18. S. F. Rahman and D. E. Day, "Properties of Refractories After Exposure to High Pressure Gases: II-Effect of Exposure Time," J. Materials for Energy Systems, Vol. 1, March 1980, p. 3.

19. A Fakhr and D. E. Day, "Properties of Refractories After Exposure to High Pressure Gases: III-Effect of Percent Saturation," J. Materials for Energy Systems, Vol. 2, Dec. 1980, p. 3.

20. A. Fakhr, S. E. Rahman, and D. E. Day, "Properties of Refractories After Exposure to High Pressure Gases: IV-Dependence Upon CO/Steam Ratio," J. Materials for Energy Systems, Vol. 3, June 1981, p. 8.

21. S. F. Rahman and D. E. Day, "Properties of Refractories After Exposure to High Pressure Gases: V-Effect of Repeated Boehmite Formation and Decomposition," J. Materials for Energy Systems, Vol. 3, No. 4, March 1982, p. 22.

22. A. Fahr, S. F. Rahman, and D. E. Day, "Properties of Refractories After Exposure to High Pressure Gases: VI-Vapor vs. Liquid Contact," J. Materials for Energy Systems, Vol. 4, No. 1, June 1982, p. 48.

23. C. R. Robbins and F. A. Mauer, "Chemical Degradation of Castable Refractories in Coal Gasification Process Environments," J. Materials for Energy Systems, Vol. 3, June 1981, p. 32.

24. L. Y. Sadler, III, H. Heystek, N. S. Raymon, and T. A. Clancy, "Refractories for Dry Ash Coal Gasifiers," U. S. Bur. Mines Report of Investigations, RI 8913, 1984.

25. R. E. Dial, "Refractories for Coal Gasification and Liquefaction," Am. Ceram. Soc. Bull., Vol. 54, No. 7, 1975, p. 640.

26. S. R. Brinkley, Jr., "Note on the Condition of Equilibrium for Systems of Many Constituents," J. Chem. Phys., Vol. 14, No. 9, 1946, p. 563.

27. S. R. Brinkley, Jr., "Calculations of the Equilibrium Composition of Systems of Many Constituents," J. Chem. Phys., Vol. 15, No. 2, 1947, p. 107.

28. W. B. White, W. M. Johnson, and G. B. Dantzig, "Equilibrium in Complex Mixtures," J. Chem. Phys, Vol. 28, No. 5, 1958, p. 751.

29. G. Eriksson, "Thermodynamic Studies of High Temperature Equilibria," Acta Chem. Scand., Vol. 25, 1971, p. 2651.

30. E. Rosen, and G. Ericksson, "Thermodynamic Studies of High Temperature Equilibria," Chemica Scripta, Vol. 4, 1973, p. 193.

31. G. Eriksson, "Thermodynamic Studies of High Temperature Equilibria," Chemica Scripta, Vol. 8, 1975, p. 100.

32. T. M. Besmann, "SOLGASMIX-PV, A Computer Program to Calculate Equilibrium Relationships in Complex Chemical Systems," ORNL/TM-5775, Contract No. W-7405-eng-26.

33. JANAF Joint Army, Navy, Air Force Thermochemical Tables, 2nd ed., 1971, NSRDS-NBS 37, US Government Printing Office: Washington, DC. See also later supplements for 1971-1981.

34. E. T. Turkdogan, "Selected Thermodynamic Functions," Physical Chemistry of High Temperature Technology, Academic Press, 1980.

35. O. Kubaschewski, E. L. Evans, and C. B. Alcok, "Metallurgical Thermochemistry," Pergamon, Oxford, 1967.

36. I. Barin and O. Knacke, "Thermochemical Properties of Inorganic Substances," Springer-Verlag, Berlin and New York, 1973.

37. I. Barin, O. Knacke, and O. Kubaschewski, "Thermochemical Properties of Inorganic Substances, Supplement," Springer-Verlag, Berlin and New York, 1977.

38. O. Kubaschewski, High Temp.-High Pressures, Vol. 4, 1972, p. 1.

39. K. K. Kelley, S. S. Todd, R. L. Orr, E. G. King, and K. R. Bonnickson, "Thermodynamic Properties of Sodium-Aluminum and Potassium-Aluminum Silicates," U. S. Bur. Mines. Report of Investigations 4955.

40. R. P. Beyer, M. J. Ferrante, R. R. Brown, and G. E. Daut, "Thermodynamic Properties of Potassium Metasilicate and Disilicate," U. S. Bur. Mines. Report of Investigations 5901.

41. R. P. Beyer, M. J. Ferrante, and R. R. Brown, "Thermodynamic Properties of $KAlO_2$," J. Chem. Thermodynamics, Vol. 12, 1980, p. 985.

42. J. W. Hastie, W. S. Horton, E. R. Plante, and D. W. Bonnell, "Thermodynamic Models of Alkali-Metal Vapor Transport in Silicate Systems," High Temp.-High Pressures, Vol. 14, 1982, p. 669.

43. B. I. Arlynk, "Determination of the Heats of Formation of a Number of Compounds by Quantitative Thermal Analysis," English translation of Zhur. Priklad. Khim., Vol. 41, No. 4, April 1968, p. 783.

44. J. T. Kummer, "β-Alumina Electrolytes," Progr. Solid State Chem., Vol. 7, 1972, p. 141.

45. Y. Y. Skolis, V. A. Levitskii, and V. M. Yanishevskii, "Thermodynamics of Binary Oxides. Thermodynamic Properties of $CaAl_4O_7$ and $CaAl_{12}O_{19}$ at High Temperatures," Russian Journal of Physical Chemistry, Vol. 55, 1981, p. 25.

46. T. C. Tiearney, Jr., and K. Natesan, "Metallic Corrosion in Simulated Low-Btu Coal-Gasification Atmosphere," J. Materials for Energy Systems, Vol. 1, March 1980, p. 13.

47. E. K. Ovechkin, L. N. Shevtsova, A. E. Voitsekhovskii, and L. V. Kuznetsova, Zh. Neorg. Khim., Vol. 16, No. 11, 1971, p. 3156; Russ. J. Inorg. Chem. (Engl. Transl.), Vol. 16, No. 11, 1971, p. 1972.

48. J. W. Hastie, E. R. Plante, D. W. Bonnell, "Alkali Vapor Transport in Coal Conversion and Combustion Systems," ACS Symposium Series, 179, p. 543; J. L. Gole and W. C. Stwalley, eds., Metal Bonding and Interactions in High Temperature Systems with Emphasis on Alkali Metals.

The vita has been removed from the scanned document